Reflection coefficients in attenuative anisotropic media

Jyoti Behura & Ilya Tsvankin
Center for Wave Phenomena, Geophysics Department, Colorado School of Mines, Golden, Colorado 80401

ABSTRACT
Reservoir rocks such as heavy oils are characterized by significant attenuation and, in some cases, attenuation anisotropy. Most existing attenuation studies are focused on plane-wave attenuation coefficients, which determine the amplitude decay along the raypath of seismic waves. Here, we discuss the influence of attenuation on PP- and PS-wave reflection coefficients for anisotropic media with main emphasis on models with VTI (transversely isotropic with a vertical symmetry axis) symmetry. Concise analytic solutions obtained by linearizing the exact plane-wave reflection coefficients are verified by numerical modeling. To make a substantial contribution to reflection coefficients, attenuation has to be strong, with the quality factor Q not exceeding 10. For such highly attenuative media, it is also necessary to take attenuation anisotropy into account if the magnitude of the Thomsen-style attenuation-anisotropy parameters is relatively large. In general, the linearized reflection coefficients in attenuative media include velocity-anisotropy parameters but have almost "isotropic" dependence on attenuation. Our formalism also helps to evaluate the influence of the inhomogeneity angle (the angle between the real and imaginary parts of the slowness vector) on the reflection coefficients. A nonzero inhomogeneity angle of the incident wave introduces additional terms into the PP- and PS-wave reflection coefficients, making conventional AVO (amplitude-variation-with-offset) analysis inadequate for strongly attenuative media. It is interesting that an incident P-wave with a nonzero inhomogeneity angle generates a mode-converted PS-wave at normal incidence, even if both halfspaces have a horizontal symmetry plane. This phenomenon can provide an alternative explanation for substantial PS-wave energy at zero offset observed on field data. The linearized solutions developed here can be used in AVO inversion for highly attenuative (e.g., gas-sand and heavy-oil) reservoirs.

Key words: Attenuation anisotropy, quality factor, AVO, reflection coefficient, inhomogeneity angle

1 INTRODUCTION

Traditionally AVO analysis has been carried out assuming the medium to be purely elastic. It is common knowledge, however, that subsurface formations are attenuative. Direct measurements using vertical seismic profiling (VSP) (Hauge, 1981; Hedlin *et al.*, 2001), well logs (Schmitt, 1999), and rock samples (Behura *et al.*, 2007; Winkler & Nur, 1982) show that attenuation and velocity dispersion can be significant, especially within hydrocarbon-saturated zones. Therefore, some failures of conventional AVO analysis can be attributed to the influence of attenuation (Luh, 1988; Samec *et al.*, 1990).

Physical-modeling experiments (Hosten *et al.*, 1987; Maultzsch *et al.*, 2003; Zhu *et al.*, 2007), rock-physics studies (Behura *et al.*, 2006; Prasad & Nur, 2003; Tao & King, 1990), and analysis of field data (Liu *et al.*, 1993; Lynn *et al.*, 1999; Vasconcelos & Jenner, 2005) show that attenuation can be directionally dependent and attenuation anisotropy often is more significant than velocity anisotropy (Arts & Rasolofosaon, 1992; Hosten *et al.*, 1987; Zhu *et al.*, 2007). Therefore, it is important to evaluate the influence of attenuation

and attenuation anisotropy on plane-wave reflection coefficients.

Reflection coefficients in isotropic as well as anisotropic attenuative media have been analyzed both analytically and using numerical modeling. For example, Krebes (1983) and Ursin & Stovas (2002) derive closed-form expressions for reflection/transmission coefficients in isotropic attenuative media, while Nechtschein & Hron (1997) and Hearn & Krebes (1990) study them numerically. For attenuative VTI media, numerical analysis of reflection/transmission coefficients are presented by Sidler & Carcione (2007). Existing results for anisotropic media, however, do not provide physical insight into the dependence of reflection/transmission coefficients on the medium properties, in particular on the anisotropy parameters.

Here, using the Thomsen-style notation introduced by Zhu & Tsvankin (2006), we develop linearized approximations for PP- and PS-wave reflection coefficients in VTI media. In particular, our analytic solutions help to evaluate the influence of the inhomogeneity angle (the angle between the real and the imaginary parts of the slowness vector) of the incident wave on the reflection coefficients. Then we compute exact reflection coefficients for a realistic range of the anisotropy parameters and assess the accuracy of the linearized expressions.

2 PERTURBATION ANALYSIS OF REFLECTION/TRANSMISSION COEFFICIENTS

For a welded contact between two arbitrary anisotropic attenuative halfspaces, the boundary conditions of the continuity of traction and displacement result in the following system of linear equations (e.g., Vavrycuk & Pšenčík, 1998):

$$\tilde{\mathbf{C}} \cdot \tilde{\mathbf{U}} = \tilde{\mathbf{B}}, \tag{1}$$

where the accent $\tilde{}$ denotes a complex quantity, $\tilde{\mathbf{C}}$ corresponds to the displacement-stress matrix for the reflected and transmitted plane waves P, S_1 and S_2, $\tilde{\mathbf{B}}$ is the displacement-stress vector of the incident wave, and $\tilde{\mathbf{U}}$ is the vector of the reflection (R) and transmission (T) coefficients. $\tilde{\mathbf{C}}$, $\tilde{\mathbf{U}}$, and $\tilde{\mathbf{B}}$ are complex quantities because the stiffness tensor in attenuative media is complex. Exact reflection/transmission coefficients ($\tilde{\mathbf{U}}$) can be computed by solving the system of equations 1 numerically.

Following Vavrycuk & Pšenčík (1998) and Jílek (2002a,b), we apply the first-order perturbation theory to a homogeneous attenuative isotropic background medium. Linearization of the boundary conditions (equation 1) yields the perturbation $\delta\tilde{\mathbf{U}}$ in the form

$$\delta\tilde{\mathbf{U}} \quad = \quad (\tilde{\mathbf{C}}^0)^{-1}(\delta\tilde{\mathbf{B}} - \delta\tilde{\mathbf{C}} \cdot \tilde{\mathbf{U}}^0)\,. \tag{2}$$

Here $\tilde{\mathbf{C}}^0$ is the displacement-stress matrix for the reflected/transmitted waves in the background medium and $\delta\tilde{\mathbf{C}}$ represents the perturbation of $\tilde{\mathbf{C}}^0$. Similarly, $\delta\tilde{\mathbf{B}}$ is the perturbation of the displacement-stress vector of the incident wave. $\tilde{\mathbf{U}}^0$, the reflection/transmission vector in the homogeneous background, is given by

$$\tilde{\mathbf{U}}^0 \quad = \quad [0,\, 0,\, 0,\, 0,\, 0,\, 1]^T\,. \tag{3}$$

A similar perturbation approach is adopted by Ursin & Stovas (2002) to derive reflection/transmission coefficients for isotropic attenuative media. (Their formalism introduces a weak contrast in parameters across the interface while keeping the perturbed upper and lower halfspaces isotropic.) The change in the slownesses and polarizations of the scattered waves, required for obtaining $\delta\tilde{\mathbf{C}}$ and $\delta\tilde{\mathbf{B}}$ in equation 2, can be computed by perturbing the isotropic background medium (Jech & Pšenčík, 1989). We extend their method, developed for purely elastic media, to attenuative models by taking attenuation in the background into account.

The density-normalized complex stiffness tensor of the perturbed medium $\tilde{a}_{ijkl}$ can be written as

$$\tilde{a}_{ijkl} \quad = \quad \tilde{a}^0_{ijkl} + \delta\tilde{a}_{ijkl}, \tag{4}$$

where $\tilde{a}^0_{ijkl}$ corresponds to the background medium and $\delta\tilde{a}_{ijkl}$ is the perturbation. The tensor $\delta\tilde{a}_{ijkl}$ is responsible for both the velocity and attenuation anisotropy of the perturbed medium. The background tensor $\tilde{a}^0_{ijkl}$ is complex:

$$\tilde{a}^0_{ijkl} \quad = \quad a^0_{ijkl} + i\, a^{0,I}_{ijkl}, \tag{5}$$

where a^0_{ijkl} and $a^{0,I}_{ijkl}$ are the real and imaginary parts of $\tilde{a}^0_{ijkl}$, respectively.

The quality-factor (Q) matrix (in the two-index Voigt notation) is defined as (e.g., Carcione, 2007)

$$Q_{ij} \quad = \quad \frac{a_{ij}}{a^I_{ij}}. \tag{6}$$

For an isotropic medium, the Q-matrix takes the form

$$Q \quad = \quad \begin{bmatrix} Q_{P0} & Q_{13} & Q_{13} & 0 & 0 & 0 \\ Q_{13} & Q_{P0} & Q_{13} & 0 & 0 & 0 \\ Q_{13} & Q_{13} & Q_{P0} & 0 & 0 & 0 \\ 0 & 0 & 0 & Q_{S0} & 0 & 0 \\ 0 & 0 & 0 & 0 & Q_{S0} & 0 \\ 0 & 0 & 0 & 0 & 0 & Q_{S0} \end{bmatrix}, \tag{7}$$

where Q_{P0} and Q_{S0} control the P- and the S-wave attenuation, respectively, and Q_{13} is the following function of Q_{P0} and Q_{S0} (Zhu & Tsvankin, 2006):

$$Q_{13} \quad = \quad Q_{P0}\frac{a_{33} - 2a_{55}}{a_{33} - 2a_{55}\frac{Q_{P0}}{Q_{S0}}}. \tag{8}$$

The Christoffel equation, which describes plane-wave propagation, can be written as

$$(\tilde{a}_{ijkl}\,\tilde{k}^2\, n_i n_l - \omega\,\delta_{jk})\,\tilde{\mathrm{g}}_j \quad = \quad 0; \tag{9}$$

$\mathbf{n}$ is the unit slowness vector, $\tilde{k}$ is the wave vector, ω is the frequency, and $\tilde{\mathbf{g}}$ is the polarization vector. In

attenuative media, $\tilde{k}$ is complex and is given by

$$\tilde{k} \quad = \quad k - i\,k^I, \tag{10}$$

where k controls the velocity and k^I the attenuation in the direction $\mathbf{n}$. The ratio of k^I to k yields the normalized attenuation coefficient $\mathcal{A}$, which defines the rate of amplitude decay per wavelength (Zhu & Tsvankin, 2006):

$$\mathcal{A} \quad = \quad \frac{k^I}{k}. \tag{11}$$

When attenuation is weak ($1/Q \ll 1$) and isotropic,

$$\mathcal{A} \quad \approx \quad \frac{1}{2Q}. \tag{12}$$

In general, the real ($\mathbf{k}$) and imaginary ($\mathbf{k}^I$) parts of the wave vector can have different orientations, and the angle ξ between them is usually called the inhomogeneity angle (Figure 1b). For $\xi = 0$, the phase direction coincides with the direction of maximum attenuation (Figure 1a), which corresponds to so called "homogeneous wave propagation."

The perturbations of the wave ($\delta\tilde{\mathbf{k}}$) and polarization ($\delta\tilde{\mathbf{g}}$) vectors, obtained by substituting the perturbed tensor $\tilde{a}_{ijkl}$ (equation 4) into the Christoffel equation 9, are used in equation 2 to derive $\delta\tilde{\mathbf{U}}$ (Jech & Pšenčík, 1989; Vavrycuk & Pšenčík, 1998; Jílek, 2002b). Note that the vector $\mathbf{n}$ in equation 9 is assumed to be real, so the perturbation analysis used here for computing $\delta\tilde{\mathbf{k}}$ and $\delta\tilde{\mathbf{g}}$ is strictly valid only for plane waves with zero inhomogeneity angle. Nevertheless, our results are applicable for small inhomogeneity angles ($< 30^\circ$) even if attenuation is strong (< 10), as will be shown later.

The complex P- and S-wave velocities ($\tilde{V}_{P0}$ and $\tilde{V}_{S0}$) in the background attenuative isotropic medium have the form

$$\tilde{V}_{P0} \quad = \quad \frac{\omega}{\tilde{k}_{P0}} \;\approx\; V_{P0}\,(1 + i\mathcal{A}_{P0}), \tag{13}$$

$$\tilde{V}_{S0} \quad = \quad \frac{\omega}{\tilde{k}_{S0}} \;\approx\; V_{S0}\,(1 + i\mathcal{A}_{S0}), \tag{14}$$

where V_{P0} and V_{S0} are the phase velocities and $\mathcal{A}_{P0}$ and $\mathcal{A}_{S0}$ are the normalized attenuation coefficients of P- and S-waves, respectively. In equations 13 and 14, terms of the second and higher order in $1/Q$ are neglected.

3 INCIDENT P-WAVE WITH ZERO INHOMOGENEITY ANGLE

If the inhomogeneity angle is set to zero, all terms in equation 2 coincide with those given in Vavrycuk & Pšenčík (1998) and Jílek (2002a,b) for non-attenuative media, but they become complex quantities. Hence, the linearized reflection coefficients for P-waves (Vavrycuk & Pšenčík, 1998) and PS-waves (Jílek, 2002a) can be adapted in a straightforward way for attenuative media.

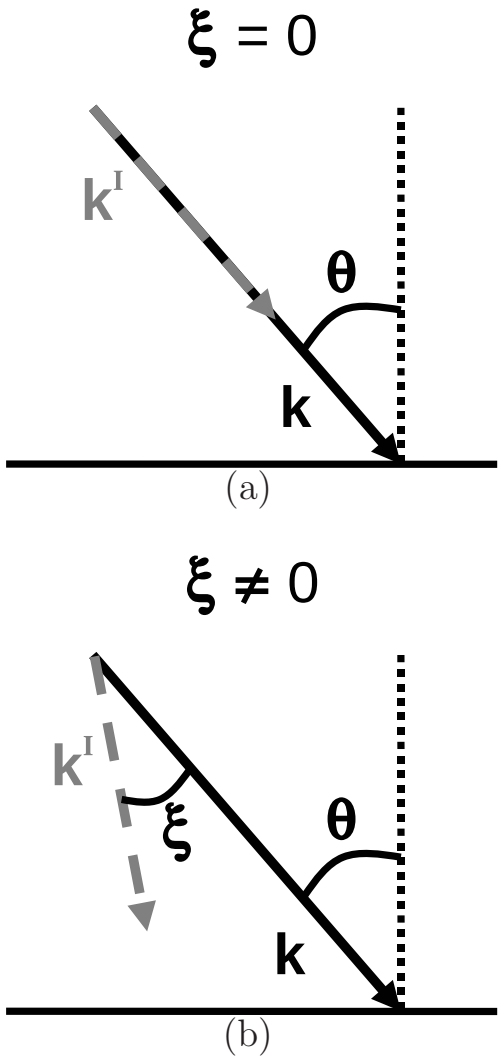

Figure 1. Incident plane wave with (a) zero inhomogeneity angle and (b) nonzero inhomogeneity angle ξ. $\mathbf{k}$ and $\mathbf{k}^I$ are the real and imaginary components (respectively) of the wave vector, and θ is the incidence phase angle.

3.1 PP-wave reflection coefficient

3.1.1 Arbitrarily anisotropic media

The linearized PP-wave reflection coefficient in arbitrarily anisotropic media obtained from equation 2 for an incident wave with zero inhomogeneity angle is given by

$$\begin{aligned} R^{\mathrm{H}}_{\mathrm{PP}} \quad = \quad & \frac{\Delta\rho}{2\rho_0} + \frac{\Delta\tilde{a}_{33}}{4\tilde{V}^2_{P0}} \\ & + \left(\frac{\Delta\tilde{a}_{13}}{2\tilde{V}^2_{P0}} - \frac{\Delta\tilde{a}_{33}}{4\tilde{V}^2_{P0}} - \frac{\Delta\tilde{a}_{55}}{\tilde{V}^2_{P0}} - \frac{2\tilde{V}^2_{S0}}{\tilde{V}^2_{P0}} \frac{\Delta\rho}{\rho_0} \right) \sin^2\theta \\ & + \frac{\Delta\tilde{a}_{11}}{4\tilde{V}^2_{P0}} \sin^4\theta, \end{aligned} \tag{15}$$

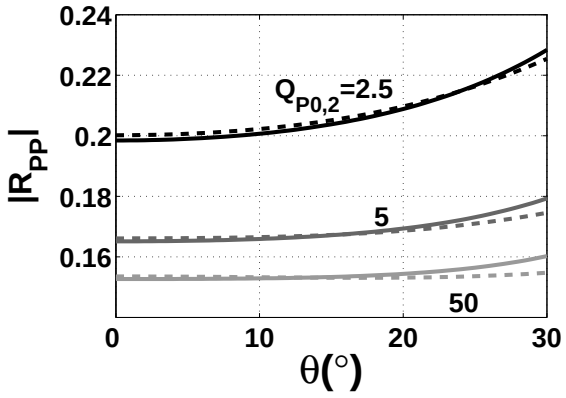

Figure 2. Magnitude of the PP-wave reflection coefficient at the ocean floor for different quality factors $Q_{P0,2}$ of the ocean-floor sediments. The solid lines are the exact coefficients and dashed lines mark the linearized approximation 16. The model parameters are listed in Table 1.

where the superscript "H" ("homogeneous") denotes an incident wave with $\xi = 0^\circ$, Δ is the contrast in a certain parameter across the interface, ρ_0 is the density of the background medium, $\tilde{a}_{ij}$ are the density-normalized complex stiffness coefficients in Voigt notation (i.e., the stiffness matrix), and θ the incidence angle (i.e., the angle between the slowness vector of the incident wave and the interface normal; Figure 1a). Equation 15 is derived under the assumption that the contrasts in the medium properties across the interface are small: $|\Delta\tilde{a}_{ijkl}| \ll \|\tilde{a}^0_{ijkl}\|, |\Delta\rho| \ll \rho^0$.

The linearized reflection coefficient in equation 15 reduces to that in purely elastic media if all parameters are made real. Thus, linearized reflection coefficients for attenuative media can be derived from those for purely elastic media by simply making the stiffnesses complex. Although equation 15 is strictly valid only for zero inhomogeneity angle (for all waves), it remains sufficiently accurate for an arbitrary inhomogeneity angle, unless the medium is strongly attenuative (as shown below).

3.1.2 VTI media

Next, we analyze equation 15 for the special case of attenuative VTI media. It is convenient to express the reflection coefficients in terms of the velocity-anisotropy and attenuation-anisotropy parameters using Thomsen-style notation. Here, we use the anisotropy parameters $\mathcal{A}_{P0}$, $\mathcal{A}_{S0}$, ϵ_Q, δ_Q, and γ_Q for attenuative TI media introduced by Zhu & Tsvankin (2006). $\mathcal{A}_{P0}$ and $\mathcal{A}_{S0}$ are the normalized symmetry-direction attenuation coefficients of P- and S-waves, respectively, ϵ_Q and δ_Q control the angular variation of the P- and SV-wave attenuation coefficients, and γ_Q governs SH-wave attenuation anisotropy.

To simplify equation 15, it is convenient to assume that terms proportional to $1/Q^2$ (but not to $1/Q$) are small. If we retain terms such as $\Delta V_{P0}/(V_P\, Q_{P0})$ and $\Delta\mathcal{A}_{P0}/Q_{P0}$ but drop those proportional to $1/Q^2_{P0}$ and $1/Q^2_{S0}$, equation 15 takes the form

$$R^{\rm H}_{\rm PP} = R^{\rm H}_{\rm PP}(0) + G^{\rm H}_{\rm PP}\sin^2\theta + C^{\rm H}_{\rm PP}\sin^4\theta, \qquad (16)$$

where $R^{\rm H}_{\rm PP}(0)$ is the normal-incidence PP-wave reflection coefficient (AVO intercept), $G^{\rm H}_{\rm PP}$ is the AVO gradient, and $C^{\rm H}_{\rm PP}$ is the curvature.

In equation 15 we retained only the quartic and lower-order terms in $\sin\theta$. Therefore, the accuracy of equation 16 somewhat decreases with incidence angle (Figure 2). Still even for $Q_{P0,2}$ as low as 2.5, the linearized approximation is close to the exact reflection coefficient for $\theta \le 30^\circ$.

Equation 16 is a Shuey-type approximation for the PP reflection coefficient in attenuative media, in which all three terms are complex:

$$R^{\rm H}_{\rm PP}(0) = \frac{\Delta\rho}{2\rho_0} + \frac{\Delta V_{P0}}{2V_{P0}} + \frac{\Delta\mathcal{A}_{P0}}{2}\left(i + \frac{1}{Q_{P0}}\right), \qquad (17)$$

$$\begin{aligned} G^{\rm H}_{\rm PP} = {} & \frac{-2}{g^2}\frac{\Delta\rho}{\rho_0} + \frac{\Delta V_{P0}}{2V_{P0}} - \frac{4}{g^2}\frac{\Delta V_{S0}}{V_{S0}} + \frac{\Delta\delta}{2} \\ & + i\left(\frac{\Delta\mathcal{A}_{P0}}{2} - \frac{4\Delta\mathcal{A}_{S0}}{g^2}\right) \\ & + \frac{i}{Q_{P0}}\left(\frac{2}{g^2}\frac{\Delta\rho}{\rho_0} + \frac{4}{g^2}\frac{\Delta V_{S0}}{V_{S0}} - \frac{i}{2}\Delta\mathcal{A}_{P0}\right. \\ & \left. + \frac{4i}{g^2}\Delta\mathcal{A}_{S0} + \frac{\Delta\delta_Q}{4}\right) \\ & - \frac{i}{Q_{S0}}\frac{2}{g^2}\left(\frac{\Delta\rho}{\rho_0} + 2\frac{\Delta V_{S0}}{V_{S0}}\right), \end{aligned} \qquad (18)$$

and

$$\begin{aligned} C^{\rm H}_{\rm PP} = {} & \frac{\Delta V_{P0}}{2V_{P0}} + \frac{\Delta\epsilon}{2} \\ & + \frac{i}{2}\Delta\mathcal{A}_{P0} + \frac{1}{Q_{P0}}\left(\frac{\Delta\mathcal{A}_{P0}}{2} + \frac{i}{4}\Delta\epsilon_Q\right); \end{aligned} \qquad (19)$$

$g \equiv V_{P0}/V_{S0}$. The contribution of the terms scaled by $1/Q_{P0}$ and $1/Q_{S0}$ in equations 17–19 is of the second order, unless attenuation is uncommonly strong.

Eliminating the influence of attenuation on $R^{\rm H}_{\rm PP}(0)$, $G^{\rm H}_{\rm PP}$, and $C^{\rm H}_{\rm PP}$ in equations 17–19 reduces them to well-known expressions for the PP-wave intercept, gradient, and curvature (respectively) for purely elastic VTI media (Rüger, 2002). Since the attenuation coefficient $\mathcal{A} \sim 1/2Q$, it is clear from equations 17–19 that the influence of attenuation on the reflection coefficient is comparable to that of the velocity and density contrasts only if the medium is strongly anelastic (i.e., $Q_{P0}, Q_{S0} < 10$). This conclusion is confirmed by the

Parameters	Fig. 2	Fig. 3	Fig. 4	Figs. 5 & 6	Fig. 8	Fig. 9
ρ_1	1.0	2.0	2.0	2.0	2.3	2.3
$V_{P0,1}$	1.5	2.0	2.0	2.0	3.3	3.3
$V_{S0,1}$	0	1.1	1.1	1.1	1.9	1.9
δ_1	0	0.2	0.2	0.2	0	0
ϵ_1	0	0.1	0.1	0.1	0	0
$Q_{P0,1}$	∞	500	500	-	5	-
$Q_{S0,1}$	∞	500	500	-	5	-
$\delta_{Q,1}$	0	0.8	0.8	0.8	0	0
$\epsilon_{Q,1}$	0	-0.4	-0.4	-0.4	0	0
ρ_2	1.2	2.0	2.0	2.0	2.0	2.0
$V_{P0,2}$	1.7	1.8	1.8	1.8	2.5	2.5
$V_{S0,2}$	0.3	1.0	1.0	1.0	1.3	1.3
δ_2	0	0	0	0	0	0.1
ϵ_2	0	0	0	0	0	0.2
$Q_{P0,2}$	-	-	-	-	5	-
$Q_{S0,2}$	50	-	-	-	50	-
$\delta_{Q,2}$	0	0	-	0	0	0.8
$\epsilon_{Q,2}$	0	0	0	0	0	-0.4

Table 1. Medium parameters used in the numerical tests. For all models, the symmetry-direction velocities (V_{P0} and V_{S0}) are in km/s and density (ρ) is in gm/cm^3.

test in Figure 3 with the model parameters simulating an interface between shale and oil sand (the shale is non-attenuative). When the oil sand is moderately attenuative ($Q_{P,2} = Q_{S,2} = 50$), the reflection coefficient is almost identical to those in the elastic case. Even a Q-value of 10 does not significantly change the reflection coefficient. However, when the attenuation is extremely strong ($Q_{P,2} = Q_{S,2} = 2.5$ or 5), the reflection coefficient substantially deviates from that for the purely elastic model.

Note that $\Delta\mathcal{A}_{P0}$ in equation 17 is responsible for the influence of attenuation on the normal-incidence reflection coefficient. In fact, the "isotropic" parameter $\Delta\mathcal{A}_{P0}$ makes a more significant contribution to $G^{\rm H}_{\rm PP}$ and $C^{\rm H}_{\rm PP}$ than do ϵ_Q and δ_Q, because the attenuation-anisotropy parameters in equations 18 and 19 are scaled by $1/Q_{P0}$.

In purely elastic anisotropic media, the linearized AVO gradient is sensitive to the velocity-anisotropy parameters (e.g., to the coefficient δ for P-waves in VTI media; see equation 18). The AVO gradient in equation 18, however, is weakly dependent on the attenuation-anisotropy parameters, unless attenuation is uncommonly strong. Although the parameter δ_Q governs the P-wave attenuation near the symmetry axis, its influence on $G^{\rm H}_{\rm PP}$ is less significant than that of δ because $\Delta\delta_Q$ is scaled by $1/Q_{P0}$. Similarly, the contribution of $\Delta\epsilon_Q$ to $C^{\rm H}_{\rm PP}$ (equation 19) is smaller than that of $\Delta\epsilon$. Because the influence of the parameter ϵ_Q increases with the incidence angle, it does not contribute to the AVO gradient.* Therefore, the reflection coefficient in media with $Q > 10$ is more influenced by velocity anisotropy than by attenuation anisotropy.

This conclusion is confirmed by Figure 4 where the model is similar to that in Figure 3, but the oil sand exhibits attenuation anisotropy. When attenuation is weak ($Q = 50$), the AVO gradient barely varies with the attenuation-anisotropy parameter δ_Q. However, as the magnitude of attenuation increases ($Q \le 10$), the influence of attenuation anisotropy becomes pronounced. Indeed, strong attenuation can even change the sign of the AVO gradient. Our results confirm the common view that moderate attenuation does not substantially distort reflection coefficients. For highly attenuative media

*The parameters γ and γ_Q only control the anisotropy of SH-waves, which are decoupled from P- and SV-waves analyzed here.

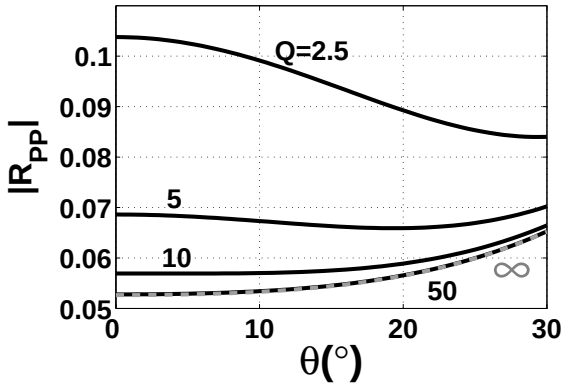

Figure 3. Exact PP-wave reflection coefficient for an interface between a non-attenuative VTI shale and isotropic attenuative oil sand (Table 1). The solid lines correspond to different Q-values in the sand ($Q = Q_{P0,2} = Q_{S0,2}$), and the gray dashed line corresponds to a non-attenuative oil sand ($Q_{P0,2} = Q_{S0,2} = \infty$).

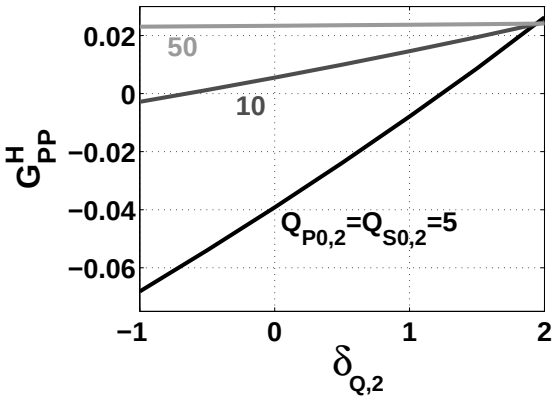

Figure 4. Exact PP-wave AVO gradient as a function of the attenuation-anisotropy parameter $\delta_{Q,2}$ in the reflecting halfspace. The model is similar to that in Figure 3, but the attenuation in the oil sand is anisotropic (Table 1).

with $Q < 10$, however, it is necessary to take not just attenuation, but also attenuation anisotropy into account.

3.2 PS-wave reflection coefficient for VTI media

Using the approach outlined above, we obtained the following closed-form linearized expression for the PS-wave reflection (conversion) coefficient in attenuative VTI media:

$$R^{\rm H}_{\rm PS} \quad = \quad B^{\rm H}_{\rm PS} \sin\theta + K^{\rm H}_{\rm PS} \sin^3\theta, \tag{20}$$

where the coefficients $B^{\rm H}_{\rm PS}$ and $K^{\rm H}_{\rm PS}$ (the gradient and curvature terms, respectively, in conventional PS-wave AVO analysis) are given by

$$\begin{aligned} B^{\rm H}_{\rm PS} \quad &= \quad -\frac{2+g}{2g}\frac{\Delta\rho}{\rho_0} - \frac{2}{g}\frac{\Delta V_{S0}}{V_{S0}} + \frac{g}{2(1+g)}\,\Delta\delta \\ &\quad -i\frac{2}{g}\,\Delta\mathcal{A}_{S0} + \frac{i}{Q_{P0}} f_1 - \frac{i}{Q_{S0}} f_2, \end{aligned} \tag{21}$$

$$\begin{aligned} K^{\rm H}_{\rm PS} \quad &= \quad \frac{(3+2g)}{4g^2}\frac{\Delta\rho}{\rho_0} + \frac{2+g}{g^2}\frac{\Delta V_{S0}}{V_{S0}} \\ &\quad +\frac{1-4g}{2(1+g)}\,\Delta\delta + \frac{g}{1+g}\,\Delta\epsilon \\ &\quad +i\frac{2+g}{g^2}\,\Delta\mathcal{A}_{S0} - \frac{i}{2Q_{P0}} f_3 + \frac{i}{2Q_{S0}} f_4. \end{aligned} \tag{22}$$

Here, f_1, f_2, f_3, and f_4 are linear combinations of the parameter contrasts across the interface listed in Appendix A. The contribution of $f_{1,2,3,4}$ to the reflection coefficient is of the second order because they are scaled by $1/Q_{P0}$ or $1/Q_{S0}$.

The real part of the reflection coefficient in equation 20 coincides with the corresponding linearized expression for PS-waves in a purely elastic VTI medium. Most conclusions drawn above for P-waves remain valid for the PS-wave reflection coefficients as well. In particular, the influence of the attenuation contrasts to $R^{\rm H}_{\rm PS}$ becomes comparable to that of the velocity and density contrasts only when $Q_{P0}, Q_{S0} \le 10$. The contribution of attenuation to $R^{\rm H}_{\rm PS}$ is controlled primarily by from the contrast in $\mathcal{A}_{S0}$ (equations 21 and 22) because $\Delta\epsilon_Q$ and $\Delta\delta_Q$ contribute only to the functions $f_{1,3}$ scaled by $1/Q_{P0}$ (equations A1 and A3).

4 INCIDENT P-WAVE WITH A NONZERO INHOMOGENEITY ANGLE

If the upper halfspace is attenuative, the incident P-wave can have a nonzero inhomogeneity angle (Figure 1b). This situation may be typical, for example, for the bottom of an attenuative reservoir. Since ξ is determined by the medium properties along the whole raypath, the imaginary part $\mathbf{k}^I$ of the wave vector of the incident wave may even deviate from the incidence plane. However, for simplicity, we assume that both the real and imaginary parts of the wave vector are confined to the incidence plane.

For a nonzero inhomogeneity angle, the Christoffel equation becomes

$$(\tilde{a}_{ijkl}\,\tilde{k}_i\,\tilde{k}_l - \omega\,\delta_{jk})\,\tilde{\mathrm{g}}_j \quad = \quad 0. \tag{23}$$

Here, the real ($\mathbf{k}$) and imaginary ($\mathbf{k}^I$) parts of $\tilde{\mathbf{k}}$ point in different directions (Figure 1b).

Although the perturbation analysis of Jech & Pšenčík (1989) is not strictly valid for equation 23, it

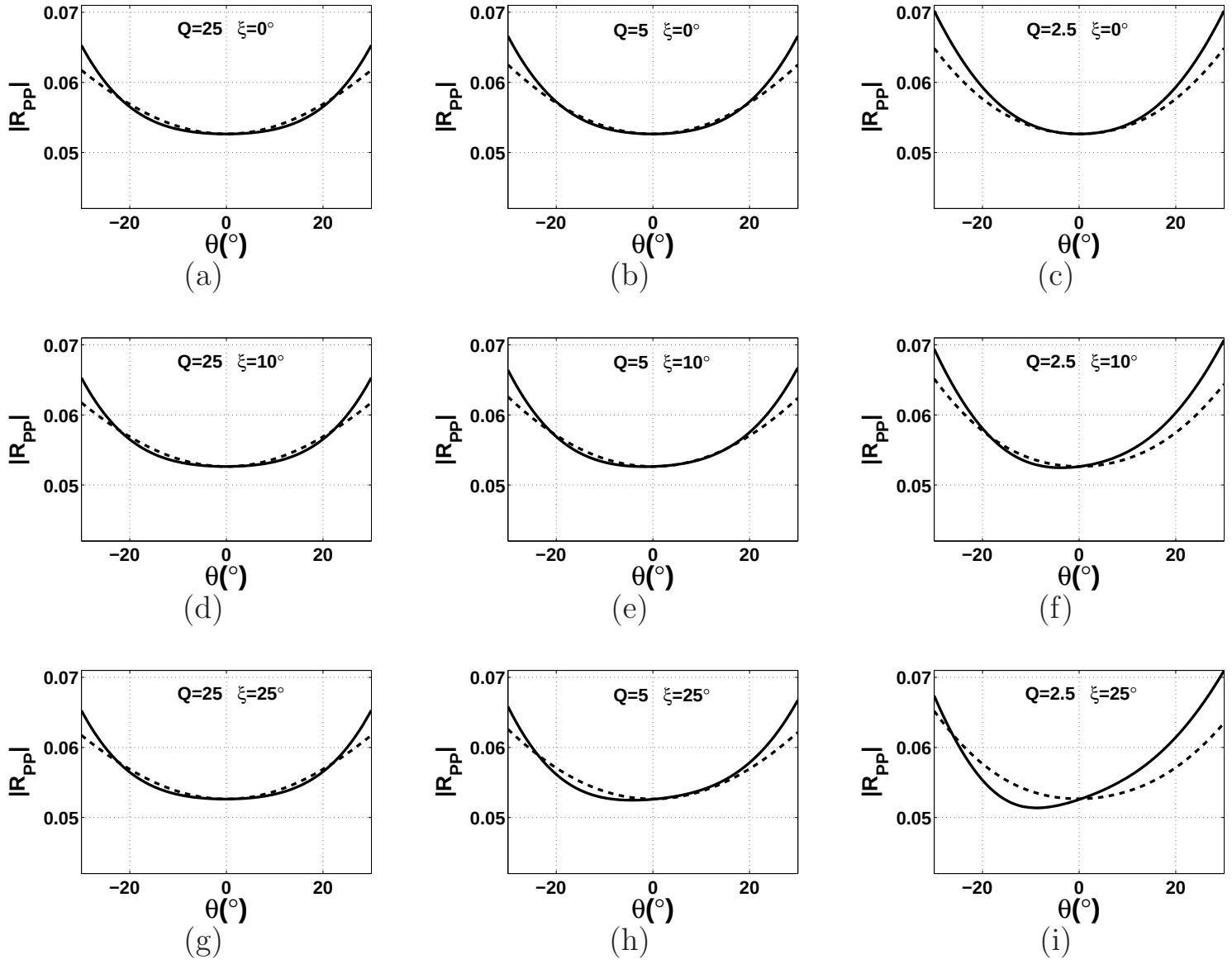

Figure 5: Magnitude of the exact (solid lines) and approximate (dashed lines, equation 25) PP-wave reflection coefficient as a VTI/isotropic interface for different inhomogeneity angles. The P- and S-wave attenuation coefficients in the vertical (symmetry-axis) direction are identical and do not change across the interface ($Q = Q_{P0,1} = Q_{P0,2} = Q_{S0,1} = Q_{S0,2}$). (a) $\xi = 0°, Q = 25$, (b) $\xi = 0°, Q = 5$, (c) $\xi = 0°, Q = 2.5$, (d) $\xi = 10°, Q = 25$, (e) $\xi = 10°, Q = 5$, (f) $\xi = 10°, Q = 2.5$, (g) $\xi = 25°, Q = 25$, (h) $\xi = 25°, Q = 5$, and (i) $\xi = 25°, Q = 2.5$. The other model parameters are listed in Table 1.

remains sufficiently accurate for small values of ξ, especially when attenuation is not strong (Zhu & Tsvankin, 2006). Therefore, the formulation of Vavrycuk & Pšenčík (1998) and Jílek (2002a,b) can be applied in a straightforward way to linearize the reflection coefficients for an incident wave with nonzero ξ. The numerical results below confirm that this approach yields an accurate approximation for reflection coefficients for most plausible attenuative models.

4.1 PP-wave reflection coefficient

The linearized PP-wave reflection coefficient for arbitrarily anisotropic media depends on the following parameters:

$$R_{\rm PP}^{\rm IH} = f_0(\Delta\rho/\rho^0, \tilde{V}_{P0}, \tilde{V}_{S0}, \Delta\tilde{a}_{11}, \Delta\tilde{a}_{13}, \Delta\tilde{a}_{15}, \Delta\tilde{a}_{33}, \Delta\tilde{a}_{35}, \Delta\tilde{a}_{55}, \theta, \xi), \quad (24)$$

where f_0 is a linear function. Due to the complicated form of f_0, it is not shown here explicitly. The reflection coefficient in equation 24 depends on three additional stiffness contrasts ($\Delta\tilde{a}_{11}, \Delta\tilde{a}_{15}$, and $\Delta\tilde{a}_{35}$) compared to that for $\xi = 0^\circ$ (equation 15).

Dropping cubic and higher-order terms in $\sin\theta$ and $\sin\xi$, we simplify the perturbation result 24 to

$$R_{\rm PP}^{\rm IH} = R_{\rm PP}^{\rm IH}(0) + B_{\rm PP}^{\rm IH}\sin\theta + G_{\rm PP}^{\rm IH}\sin^2\theta, \quad (25)$$

where

$$R_{\rm PP}^{\rm IH}(0) = R_{\rm PP}^{\rm H}(0) + \frac{\sin^2\xi}{4Q_{P0}} f_5, \quad (26)$$

$$B_{\rm PP}^{\rm IH} = \frac{-i\sin\xi}{Q_{P0}} f_6, \quad (27)$$

$$G_{\rm PP}^{\rm IH} = G_{\rm PP}^{\rm H} + \frac{i\sin^2\xi}{8Q_{P0}} f_7. \quad (28)$$

Here, $R_{\rm PP}^{\rm H}(0)$ and $G_{\rm PP}^{\rm H}$ are the solutions for $\xi = 0^\circ$ (superscript "H") given by equations 17 and 18, respectively, and f_5, f_6, and f_7 are linear functions listed in Appendix A.

As illustrated by Figure 5, equation 25 remains accurate for the inhomogeneity angle as large as 25°. Even for $Q = 2.5$ and $\xi = 25^\circ$, (Figure 5i), approximation 25 deviates from the exact reflection coefficient by less than 10%.

In contrast to the conventional AVO equation for non-converted waves, which represents an even function of θ (e.g., equation 16), equation 25 includes the $\sin\theta$-term. Therefore, if attenuation is strong and the inhomogeneity angle ξ is non-negligible, the basic equation of conventional PP-wave AVO analysis breaks down, which may have significant implications for AVO inversion and interpretation.

However, since the inhomogeneity angle ξ is associated with the terms f_5, f_6, and f_7, which are scaled by

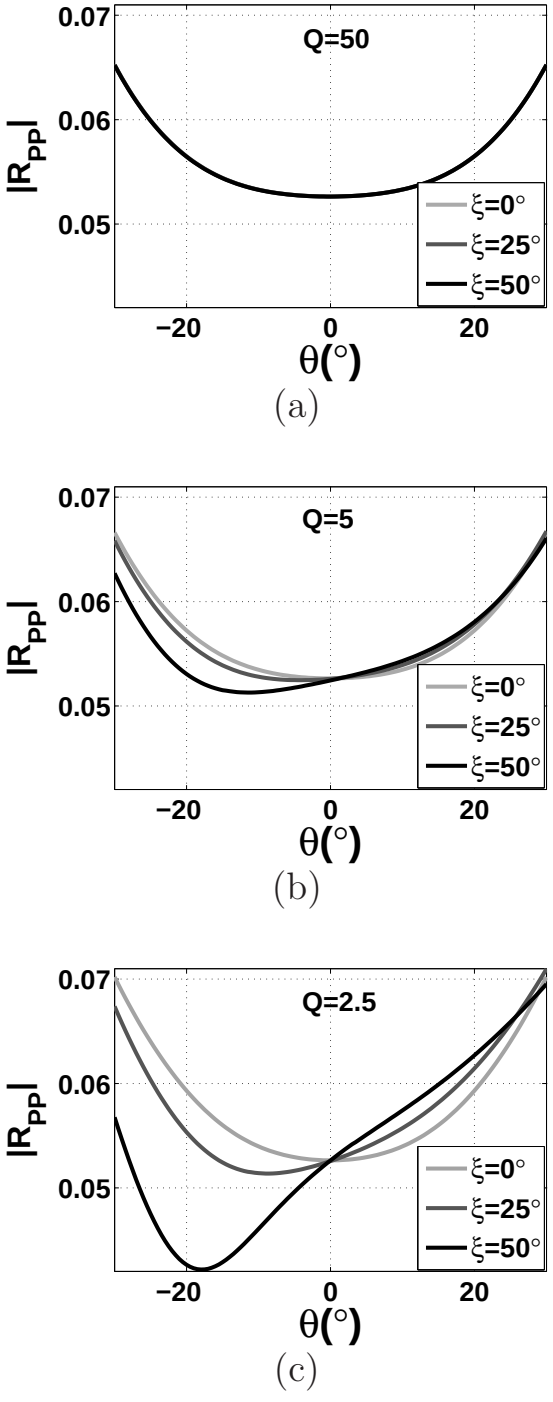

Figure 6. Magnitude of the exact PP-wave reflection coefficient at a VTI/isotropic interface for different inhomogeneity angles. As in Figure 5, $Q = Q_{P0,1} = Q_{P0,2} = Q_{S0,1} = Q_{S0,2}$; (a) $Q = 50$, (b) $Q = 5$, and (c) $Q = 2.5$. The other model parameters are listed in Table 1.

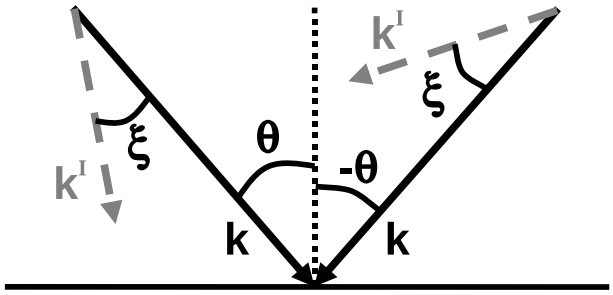

Figure 7. PP-wave reflection coefficient may become asymmetric with respect to $\theta = 0^\circ$ for a nonzero inhomogeneity angle ξ. As before, $\mathbf{k}$ and $\mathbf{k}^I$ are the real and imaginary parts, respectively, of the wave vector of the incident P-wave.

$1/Q$, its influence becomes pronounced only in strongly attenuative media. As illustrated in Figure 6, the variation of the inhomogeneity angle from 0° to 50° does not significantly change the reflection coefficient even for $Q = 5$ (Figure 6b). Only when $Q = 2.5$ and the inhomogeneity angle exceeds 30°, its contribution to the reflection coefficient (in particular, to the term $B^{\rm IH}_{\rm PP}$) becomes substantial (Figure 6c).

The asymmetry of the reflection coefficient with respect to $\theta = 0^\circ$ (Figures 6b and 6c), which increases with the inhomogeneity angle, is explained in Figure 7. In our modeling, the inhomogeneity angle of the incident wave is fixed, which implies that the imaginary part $\mathbf{k}^I$ of the wave vector makes different angles with the vertical for the incidence angles θ and $-\theta$. As a result, the reflection coefficient for positive and negative incidence angles is not the same.

In reality, it is unlikely for the incident wave to have a constant inhomogeneity angle for a wide range of θ. A more plausible scenario is depicted in Figure 8a. The model includes an attenuative reservoir beneath a purely elastic cap rock. Because the cap rock is purely non-attenuative, the wave incident upon the reservoir has a real wave vector. According to Snell's law, the horizontal slowness (and the horizontal component of the wave vector) has to be preserved during reflection and transmission. Therefore, the vector $\mathbf{k}^I$ (the imaginary part of $\tilde{\mathbf{k}}$) in the reservoir cannot have a horizontal component, and the inhomogeneity angle of the transmitted wave is equal to the transmission angle θ_T (Figure 8a). For the reflection from the bottom of the reservoir, θ_T becomes the incidence angle. Therefore, the wave vectors $\mathbf{k}$ and $\mathbf{k}^I$ for the angles θ_T and $-\theta_T$ are symmetric with respect to the reflector normal, and the PP-wave reflection coefficient is an even function of θ (Figure 8b, gray line). However, for more complicated overburden models, the inhomogeneity angle can be different from the incidence angle, which makes the reflection coefficient asymmetric with respect to θ (Figure 8b, black line; $\xi = 50^\circ$ was held constant).

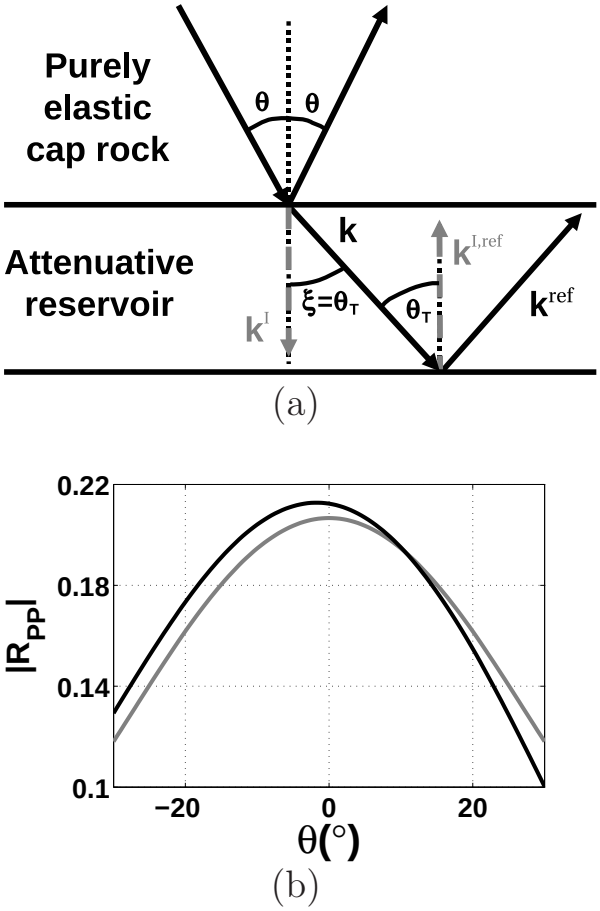

Figure 8. (a) Wave vector of a plane wave in an attenuative medium (reservoir) overlaid by a purely elastic medium (cap rock). The transmission angle θ_T is equal to the inhomogeneity angle ξ of the transmitted wave. $\mathbf{k}^{ref}$ and $\mathbf{k}^{I,ref}$ are the real and imaginary components, respectively, of the wave vector for the reflection from the bottom of the attenuative layer. (b) Exact PP-wave reflection coefficient from the bottom of the attenuative layer for $\xi = \theta_T$ (gray line, Figure 8a) and for a constant inhomogeneity angle $\xi = 50^\circ$ (black line). The model parameters are listed in Table 1.

4.2 PS-wave reflection coefficient

As is the case for PP-waves, the inhomogeneity angle of the incident P-wave changes the conventional PS-wave AVO equation. The linearized PS-wave coefficient takes the form

$$R^{\rm IH}_{\rm PS} = R^{\rm IH}_{\rm PS}(0) + B^{\rm IH}_{\rm PS}\sin\theta + G^{\rm IH}_{\rm PS}\sin^2\theta, \qquad (29)$$

where

$$R^{\rm IH}_{\rm PS}(0) = i\frac{\sin\xi}{Q_{P0}}f_8, \qquad (30)$$

$$B^{\rm IH}_{\rm PS} = B^{\rm H}_{\rm PS}, \qquad (31)$$

$$G_{\rm PS}^{\rm IH} \quad = \quad -i\frac{\sin\xi}{Q_{P0}}f_9. \tag{32}$$

In equations 29–32, cubic and higher-order terms in $\sin\theta$ and $\sin\xi$ are neglected. $B_{\rm PS}^{\rm H}$ is the PS-wave AVO gradient for an incident wave with zero inhomogeneity angle (equation 21), and the terms f_8 and f_9 are linear combinations of the parameter contrasts across the interface (Appendix A).

Equation 29 is different from equation 20 for $\xi = 0^\circ$, in which only the coefficients of odd powers in $\sin\theta$ are nonzero (i.e., the reflection coefficient is an odd function of θ). The deviation of equation 29 from the conventional PS-wave AVO equation is illustrated in Figure 9, where the magnitude of the PS-wave reflection coefficient in strongly attenuative media ($Q = 2.5$) for $\xi = 50^\circ$ is visibly asymmetric with respect to $\theta = 0^\circ$. Also, for $Q < 10$ $R_{\rm PS}^{\rm IH}$ significantly deviates from the reflection coefficient for a purely elastic medium, which almost coincides with that for $Q = 50$.

Because the linearized AVO gradient $B_{\rm PS}^{\rm IH}$ is independent of ξ (for small ξ), the inhomogeneity angle has a greater influence on $R_{\rm PS}^{\rm IH}(0)$ and $G_{\rm PS}^{\rm IH}$ than on $B_{\rm PS}^{\rm IH}$. For zero inhomogeneity angle of the incident wave, $R_{\rm PS}^{\rm IH}(0)$ and $G_{\rm PS}^{\rm IH}$ vanish and equation 29 reduces to equation 20 (ignoring the cubic term in $\sin\theta$) discussed above.

For $\xi \neq 0$, the normal-incidence PS-wave reflection coefficient $R_{\rm PS}^{\rm IH}$ in strongly attenuative media can attain substantial values (Figure 9). Nonzero PS-wave amplitude at normal incidence can also be caused by such factors as lateral heterogeneity, the influence of additional terms of the ray-series expansion on point-source radiation (Tsvankin, 1995), and the deviation of the reflector from the symmetry planes of the model (Behura & Tsvankin, 2006). However, we consider only plane-wave reflection coefficients and the model in Figure 9 is composed of homogeneous VTI halfspaces with a common horizontal symmetry plane. A nonzero inhomogeneity angle of the vertically travelling P-wave makes its wave vector asymmetric with respect to the reflector normal, which generates the PS conversion.

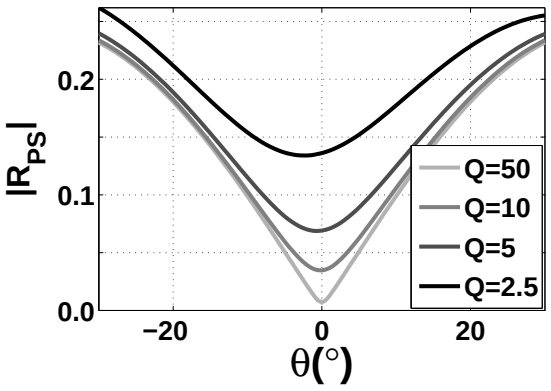

Figure 9. Magnitude of the exact PS-wave reflection coefficient at an isotropic/VTI interface for a nonzero inhomogeneity angle ($\xi = 50^\circ$) of the incident P-wave and variable quality factor $Q = Q_{P0,1} = Q_{P0,2} = Q_{S0,1} = Q_{S0,2}$. The model parameters are listed in Table 1.

5 CONCLUSIONS

We analyzed the PP- and PS-wave reflection coefficients in attenuative anisotropic media using linearized approximations verified by exact numerical modeling. For an incident P-wave with zero inhomogeneity angle, the form of the linearized PP- and PS-wave reflection coefficients is the same as that in purely elastic media, but all terms become complex. The general solutions for arbitrarily anisotropic media were simplified for VTI symmetry to obtain simple closed-form expressions in Thomsen-style notation.

Both analytic and numerical results show that only in the presence of strong attenuation ($Q < 10$) does the contribution of the imaginary part of the stiffness tensor (which is responsible for attenuation) become comparable to that of the real part. In particular, the influence of the attenuation-anisotropy parameters $\epsilon_{_Q}$ and $\delta_{_Q}$ on reflection coefficients typically is much weaker than that of the velocity-anisotropy parameters ϵ and δ. As expected from the parameter definitions, $\delta_{_Q}$ contributes to the AVO gradient (i.e., to the reflection coefficient at small incidence angles), while the influence of $\epsilon_{_Q}$ increases with incidence angle. The largest attenuation terms in the reflection coefficients for both PP- and PS-waves are proportional to the contrasts in the normalized symmetry-direction attenuation coefficients $\mathcal{A}_{P0}$ and $\mathcal{A}_{S0}$ because the contrasts in the attenuation-anisotropy parameters are scaled by $1/Q_{P0}$. Therefore, for AVO analysis in strongly attenuative media ($Q < 10$), it is sufficient to take the influence of $\mathcal{A}_{P0}$ and $\mathcal{A}_{S0}$ into account, while in media with exceptionally strong attenuation ($Q < 5$), it is necessary to consider the influence of $\epsilon_{_Q}$ and $\delta_{_Q}$ as well.

If the incident wave has a nonzero inhomogeneity angle ξ, the form of the linearized reflection coefficients is different from the conventional AVO expression. In particular, the PP-wave reflection coefficient depends on $\sin\theta$ and $\sin^3\theta$ and is no longer an even function of θ. Likewise, the PS-wave reflection coefficient at normal incidence does not vanish for $\xi \neq 0^\circ$ and may even attain substantial values. However, the contribution of the inhomogeneity angle to the AVO response becomes significant only in media with anomalously high attenuation (such as heavy-oil-saturated rocks) with $Q < 5$.

Despite the presence of attenuation-related terms, our linearized AVO equations have an easily interpretable form that provides useful physical insight into the reflectivity of anisotropic attenuative media. Their application can help to avoid errors in AVO analysis

and, potentially, invert prestack reflection amplitudes for the attenuation parameters.

6 ACKNOWLEDGMENTS

We are grateful to members of the A(nisotropy)-Team of the Center for Wave Phenomena (CWP), Colorado School of Mines for helpful discussions. The support for this work was provided by the Consortium Project on Seismic Inverse Methods for Complex Structures at CWP and the Petroleum Research Fund of the American Chemical Society.

References

Arts, R. J., & Rasolofosaon, P. N. J. 1992. Approximation of velocity and attenuation in general anisotropic rocks. *SEG Technical Program Expanded Abstracts*, **11**(1), 640–643.

Behura, J., & Tsvankin, I. 2006. Small-angle AVO response of PS-waves in tilted transversely isotropic media. *Geophysics*, **71**(5), C69–C79.

Behura, J., Batzle, M., & Hofmann, R. 2006. Shear properties of oil shales. *SEG Technical Program Expanded Abstracts*, **25**(1), 1973–1977.

Behura, J., Batzle, M., Hofmann, R., & Dorgan, J. 2007. Heavy oils: Their shear story. *Geophysics*, **72**(5), E175–E183.

Carcione, J. M. 2007. *Wave Fields in Real Media: Wave Propagation in Anisotropic, Anelastic, Porous and Electromagnetic Media*. 2nd edn. Elsevier Science.

Hauge, P. S. 1981. Measurements of attenuation from vertical seismic profiles. *Geophysics*, **46**(11), 1548–1558.

Hearn, D. J., & Krebes, E. S. 1990. On computing ray-synthetic seismograms for anelastic media using complex rays. *Geophysics*, **55**(Apr.), 422–432.

Hedlin, K., Mewhort, L., & Margrave, G. 2001. Delineation of steam flood using seismic attenuation. *SEG Technical Program Expanded Abstracts*, **20**(1), 1572–1575.

Hosten, B., Deschamps, M., & Tittmann, B. R. 1987. Inhomogeneous wave generation and propagation in lossy anisotropic solids. Application to the characterization of viscoelastic composite materials. *The Journal of the Acoustical Society of America*, **82**(Nov.), 1763–1770.

Jech, J., & Pšenčík, I. 1989. First-order perturbation method for anisotropic media. *Geophysical Journal International*, **99**, 369–376.

Jílek, P. 2002a. Converted PS-wave reflection coefficients in weakly anisotropic media. *Pure and Applied Geophysics*, **159**, 1527–1562.

Jílek, P. 2002b. *Modeling and inversion of converted-wave reflection coefficients in anisotropic media: A tool for quantitative AVO analysis*. Ph.D. thesis, Colorado School of Mines.

Krebes, E. S. 1983. The viscoelastic reflection/transmission problem: Two special cases. *Bulletin of Seismological Society of America*, **73**(Dec.), 1673–1683.

Liu, E., Crampin, S., Queen, J., & Rizer, W. 1993. Velocity and attenuation anisotropy caused by microcracks and macrofractures in a multiazimuth reverse VSP. *Canadian Journal of Exploration Geophysics*, **29**, 177–188.

Luh, P. C. 1988. Wavelet dispersion and bright spot detection. *SEG Technical Program Expanded Abstracts*, **7**(1), 1217–1220.

Lynn, H. B., Campagna, D., Simon, K. M., & Beckham, W. E. 1999. Relationship of P-wave seismic attributes, azimuthal anisotropy, and commercial gas pay in 3-D P-wave multiazimuth data, Rulison Field, Piceance Basin, Colorado. *Geophysics*, **64**(4), 1293–1311.

Maultzsch, S., Chapman, M., Liu, E., & Li, X. Y. 2003. Modelling frequency-dependent seismic anisotropy in fluid-saturated rock with aligned fractures: implication of fracture size estimation from anisotropic measurements. *Geophysical Prospecting*, **51**, 381–392.

Nechtschein, S., & Hron, F. 1997. Effects of anelasticity on reflection and transmission coefficients. *Geophysical Prospecting*, **45**, 775–793.

Prasad, M., & Nur, A. 2003. Velocity and attenuation anisotropy in reservoir rocks. *SEG Technical Program Expanded Abstracts*, **22**(1), 1652–1655.

Rüger, A. 2002. *Reflection Coefficients and Azimuthal AVO Analysis in Anisotropic Media*. Society of Exploration Geophysicists.

Samec, P., Blangy, J. P., & Nur, A. 1990. Effect of viscoelasticity and anisotropy on amplitude-versus-offset interpretation. *SEG Technical Program Expanded Abstracts*, **9**(1), 1479–1482.

Schmitt, D. R. 1999. Seismic attributes for monitoring of a shallow heated heavy oil reservoir: A case study. *Geophysics*, **64**(2), 368–377.

Sidler, R., & Carcione, J. M. 2007. Wave reflection at an anelastic transversely isotropic ocean bottom. *Geophysics*, **72**, SM139–SM146.

Tao, G., & King, M. S. 1990. Shear-wave velocity and Q anisotropy in rocks: A laboratory study. *International Journal of Rock Mechanics and Mining Science & Geomechanics Abstracts*, **27**(Oct.), 353–361.

Tsvankin, I. 1995. *Seismic wavefields in layered isotropic media*. Samizdat Press.

Ursin, B., & Stovas, A. 2002. Reflection and transmission responses of a layered isotropic viscoelastic medium. *Geophysics*, **67**(1), 307–323.

Vasconcelos, I., & Jenner, E. 2005. Estimation of azimuthally varying attenuation from wide-azimuth P-wave data. *SEG Technical Program Expanded Abstracts*, **24**(1), 123–126.

Vavrycuk, V., & Pšenčík, I. 1998. PP-wave reflection coefficients in weakly anisotropic elastic media. *Geophysics*, **63**(6), 2129–2141.

Winkler, K. W., & Nur, A. 1982. Seismic attenuation: Effects of pore fluids and frictional-sliding. *Geophysics*, **47**(1), 1–15.

Zhu, Y., & Tsvankin, I. 2006. Plane-wave propagation in attenuative transversely isotropic media. *Geophysics*, **71**(2), T17–T30.

Zhu, Y., Tsvankin, I., Dewangan, P., & van Wijk, K. 2007. Physical modeling and analysis of P-wave attenuation anisotropy in transversely isotropic media. *Geophysics*, **72**(1), D1–D7.

APPENDIX A: LINEAR FUNCTIONS IN THE APPROXIMATE REFLECTION COEFFICIENTS

Here, we give explicit expressions for the linear functions f_i in the approximate equations for the reflection coefficients.

The functions f_1, f_2, f_3, and f_4 in equations 21 and 22 have the form

$$f_1 = \frac{1}{2g}\frac{\Delta\rho}{\rho_0} + \frac{1}{g}\frac{\Delta V_{S0}}{V_{S0}} + \frac{g}{4(1+g)^2}\Delta\delta + \frac{i}{g}\Delta\mathcal{A}_{S0} + \frac{g}{4(1+g)}\Delta\delta_Q, \tag{A1}$$

$$f_2 = \frac{1}{2g}\frac{\Delta\rho}{\rho_0} + \frac{1}{g}\frac{\Delta V_{S0}}{V_{S0}} + \frac{g}{4(1+g)^2}\Delta\delta + \frac{i}{g}\Delta\mathcal{A}_{S0}, \tag{A2}$$

$$f_3 = \frac{3+g}{2g^2}\frac{\Delta\rho}{\rho_0} + \frac{4+g}{g^2}\frac{\Delta V_{S0}}{V_{S0}} - \frac{g}{(1+g)^2}\Delta\epsilon + \frac{5g}{4(1+g)^2}\Delta\delta + i\frac{4+g}{g^2}\Delta\mathcal{A}_{S0} - \frac{g}{(1+g)^2}\Delta\epsilon_Q + \frac{4g-1}{4(1+g)}\Delta\delta_Q, \tag{A3}$$

$$f_4 = \frac{3+g}{2g^2}\frac{\Delta\rho}{\rho_0} + \frac{4+g}{g^2}\frac{\Delta V_{S0}}{V_{S0}} - \frac{g}{(1+g)^2}\Delta\epsilon + \frac{5g}{4(1+g)^2}\Delta\delta + i\frac{1}{g^2}\Delta\mathcal{A}_{S0}, \tag{A4}$$

where $g \equiv V_{P0}/V_{S0}$.

The functions f_5, f_6, and f_7 in equations 26–28 are given by

$$f_5 = -i\frac{\Delta V_{P0}}{V_{P0}} + \Delta\mathcal{A}_{P0}, \tag{A5}$$

$$f_6 = \frac{-2}{g^2}\frac{\Delta\rho}{\rho_0} + \frac{\Delta V_{P0}}{2V_{P0}} - \frac{4}{g^2}\frac{\Delta V_{S0}}{V_{S0}} + \frac{\Delta\delta}{2} + i\left(\frac{\Delta\mathcal{A}_{P0}}{2} - \frac{4\Delta\mathcal{A}_{S0}}{g^2}\right), \tag{A6}$$

$$f_7 = \left(1+\frac{1}{g^2}\right)\frac{\Delta V_{P0}}{V_{P0}} - \Delta\delta + i\left(1+\frac{1}{g^2}\right)\Delta\mathcal{A}_{P0}. \tag{A7}$$

Finally, f_8 and f_9 in equations 30 and 32 are

$$f_8 = \frac{2+g}{4g}\frac{\Delta\rho}{\rho_0} + \frac{\Delta V_{S0}}{gV_{S0}} - \frac{g}{4(1+g)}\Delta\delta + \frac{i}{g}\Delta\mathcal{A}_{S0}, \tag{A8}$$

$$f_9 = \frac{9+8g+g^2}{8g^2}\frac{\Delta\rho}{\rho_0} + \frac{3+2g}{g^2}\frac{\Delta V_{S0}}{V_{S0}} + \frac{3-13g}{8(1+g)}\Delta\delta + \frac{3g}{2(1+g)}\Delta\epsilon + i\,\frac{3+2g}{g^2}\Delta\mathcal{A}_{S0}. \tag{A9}$$